Stepwise gating of the Sec61 protein-conducting channel by Sec63 and Sec62

Samuel Itskanov[1], Katie M. Kuo[2], James C. Gumbart[2,3], and Eunyong Park[4,*]

[1]Biophysics Graduate Program, University of California, Berkeley, Berkeley, CA 94720, USA.
[2]School of Chemistry and Biochemistry, Georgia Institute of Technology, Atlanta, GA 30332, USA.
[3]School of Physics, Georgia Institute of Technology, Atlanta GA 30332, USA.
[4]Department of Molecular and Cell Biology and California Institute for Quantitative Biosciences, University of California, Berkeley, Berkeley, CA 94720, USA.

[*]Corresponding author. Email: eunyong_park@berkeley.edu

Abstract

Many proteins are transported into the endoplasmic reticulum by the universally conserved Sec61 channel. Post-translational transport requires the two additional proteins Sec62 and Sec63, but their functions are poorly defined. Here, we determined cryo-electron microscopy structures of several variants of the fungal Sec61-Sec62-Sec63 complexes and show that Sec62 and Sec63 induce opening of the Sec61 channel. Without Sec62, the translocation pore of Sec61 remains closed by the plug domain, rendering the channel inactive. We further show that the lateral gate of Sec61 must be first partially opened by interactions between Sec61 and Sec63 in cytosolic and lumenal domains, a simultaneous disruption of which completely closes the channel. The structures and molecular dynamics simulations suggest that Sec62 may also prevent lipids from invading into the channel through the open lateral gate. Our study illuminates how Sec63 and Sec62 work together in a hierarchical manner to activate Sec61 for post-translational protein translocation.

Main text

In all organisms, about one third of proteins are transported across or integrated into a membrane upon synthesis by the ribosome. The majority of these translocation processes occur in the endoplasmic reticulum (ER) membrane in eukaryotes or the plasma membrane in prokaryotes, mediated by the conserved heterotrimeric protein-conducting channel called the Sec61 (SecY in prokaryotes) complex{Rapoport, 2017 #77;Voorhees, 2016 #3;Collinson, 2015 #76;Tsirigotaki, 2017 #80;Seinen, 2019 #81}. The main α subunit of the channel, comprised of ten transmembrane helices (TMs), forms an hourglass-shaped cavity, through which polypeptides are transported as extended chains. The small β and γ subunits peripherally associate with the α subunit in the membrane{Van den Berg, 2004 #1}. Previous structures of Sec61/SecY showed that in the idle state the pore is blocked in the ER lumenal (or extracellular) funnel by the plug domain—a structure formed by a segment immediately following TM1 of the α subunit{Van den Berg, 2004 #1;Tsukazaki, 2008 #21;Voorhees, 2014 #23;Tanaka, 2015 #73}, whereas in translocating states the plug moves away{Li, 2016 #40;Voorhees, 2016 #41;Ma, 2019 #70}. Sec61/SecY can also release polypeptides to the lipid phase through a gap (lateral gate) formed between TM2 and TM7 of the α subunit. The opening of the lateral gate is required for recognition of hydrophobic targeting signals (signal sequences) of soluble secretory proteins and integration of transmembrane proteins. Thus, the channel is gated in two directions: vertically across the membrane by the plug domain

and laterally within the membrane by the lateral gate. How these gates are controlled and how they regulate the translocation processes remain incompletely understood.

The Sec61/SecY channel alone is inactive and thus must associate with a partner to enable translocation. In the co-translational mode, common in both prokaryotes and eukaryotes, The channel directly docks with the ribosome-nascent-chain complex{Voorhees, 2016 #41;Braunger, 2018 #44;Gogala, 2014 #87}. Many secretory proteins are targeted to the channel post-translationally after their release from the ribosome{Ng, 1996 #5;Muller, 1987 #7;Lakkaraju, 2012 #6;Chen, 1985 #94;Cabelli, 1988 #79;Brundage, 1990 #93}. In bacteria, a single cytosolic ATPase called SecA binds to the SecY complex to drive post-translational translocation{Cabelli, 1988 #79;Brundage, 1990 #93;Zimmer, 2008 #22;Li, 2016 #40;Ma, 2019 #70}. In eukaryotes, post-translational translocation is enabled by association between the Sec61 complex and the two essential integral membrane proteins Sec62 and Sec63, forming a machinery called the Sec complex{Rothblatt, 1989 #9;Deshaies, 1991 #8;Meyer, 2000 #10;Tyedmers, 2000 #11}. In fungal species, the Sec complex also contains the additional nonessential proteins Sec71 and Sec72, which are bound to Sec63 in the cytosol. In the ER lumen, Sec63 recruits the Hsp70 ATPase BiP to the complex to power translocation{Feldheim, 1992 #13;Matlack, 1999 #17}.

Recently, two cryo-EM studies reported structures of the Sec complex from *Saccharomyces cerevisiae* at ~4 Å resolution{Itskanov, 2019 #69;Wu, 2019 #71}, which suggested a putative role of Sec63 in activating the Sec61 channel for translocation by opening the lateral gate of the channel. However, in both structures, Sec62 was barely visible, and thus its function remains unknown despite its essentiality. Furthermore, the two structures displayed noticeable conformational differences in Sec61, despite essentially identical specimen compositions. Most notably, in one structure the pore is blocked by the plug domain{Wu, 2019 #71}, whereas in the other structure the plug is displaced leaving the pore open{Itskanov, 2019 #69}. Although deemed important given the role of the plug domain in channel gating, the cause of this difference remains a puzzle. Finally, although Sec63 has been suggested to open the lateral gate of Sec61{Itskanov, 2019 #69;Wu, 2019 #71}, the mechanism of opening remains speculative without structures of mutants and other conformations. Thus, whether and how Sec62 and Sec63 regulate the function of Sec61 are poorly understood. Addressing these issues is essential for our understanding of eukaryotic post-translational translocation and the mechanism of the Sec61/SecY channel in general. Mutations in Sec61 and Sec63 have been implicated in hyperuricemic nephropathy{Bolar, 2016 #90}, diabetes{Lloyd, 2010 #91}, and polycystic liver disease{Davila, 2004 #92}.

Here, using cryo-EM, we analyzed several variants and mutants of the Sec complex from two fungal species, *Saccharomyces cerevisiae* and *Thermomyces lanuginosus*. We show that Sec62 and Sec63 cooperate to open both the lateral and vertical gates of the Sec61 channel. The structures and molecular dynamics (MD) simulations also suggest that Sec62 performs an additional function of preventing lipids from invading into the channel through the open lateral gate. Our study provides a detailed mechanistic model for how Sec62 and Sec63 activate the Sec61 channel for post-translational protein translocation in eukaryotes.

Cryo-EM analysis of two fungal Sec complexes

To determine how the gating of the Sec61 channel is regulated in the Sec complex, we first analyzed a large cryo-EM dataset of the wildtype (WT) Sec complex from *S. cerevisiae* (*Sc*Sec) (Fig. 1a,b, Table 1, and Extended Data Fig. 1). While reconstruction from approximately 1 million particles yielded a 3.0-Å-resolution consensus map (Extended Data Fig. 1b–d), we found that the particle set contained

subpopulations lacking Sec62 or Sec71-Sec72, despite apparent sample homogeneity (Extended Data Fig. 1a). We therefore performed additional three-dimensional (3D) classifications to separate particles with and without Sec62 (referred to as Sec62+ and Sec62−) (Extended Data Fig. 1b,e). Furthermore, the Sec62+ class could be further separated into two distinct subclasses (referred to as C1 and C2), which show notable conformational differences in Sec62, the lateral gate, and the plug (Fig 1b and Extended Data Fig. 1f,g; see below). The three structures (i.e., Sec62−, C1, and C2) were resolved at overall resolutions of 3.1–3.2 Å. Although an atomic model for Sec62 could not be built due to insufficient local resolution, the classification significantly improved Sec62 features, enabling unambiguous assignment of individual domains (Fig. 1d).

To gain insights into structural and mechanistic conservation across species, we also purified the Sec complex from the thermophilic fungus *T. lanuginosus* (*Tl*Sec) and determined its structures at overall resolutions of 3.6 to 3.9 Å (Fig. 1c, Table 1, and Extended Data Fig. 2). Recombinant expression of the *Tl*Sec complex allowed us to analyze complexes completely lacking Sec62 (ΔSec62 *Tl*Sec) or containing a mutant Sec62 copy for structural comparisons. Like WT *Sc*Sec, the WT *Tl*Sec dataset yielded two classes with and without Sec62 (referred to as *Tl*Sec[Sec62+] and *Tl*Sec[Sec62−]), which closely resemble the *Sc*Sec [C2] and [Sec62−] structures, respectively (brackets denote classes). We could not find a C1-equivalent class from the *Tl*Sec dataset perhaps because the specimen freezing condition (4°C) might have biased the conformation distribution of this thermophilic complex towards C2. The structure of *Tl*Sec[Sec62−] was found to be essentially identical to a separately determined structure of ΔSec62 *Tl*Sec, validating our approach to separate distinct subpopulations of the Sec complexes by cryo-EM image analysis (Extended Data Fig. 2g–i). Importantly, the domain arrangement of *Tl*Sec62 is the same as that of *Sc*Sec62 despite ~30% overall sequence identity (Fig. 1c and Supplementary Fig. 1). This corroborates the conserved architecture of Sec62. Compared to *Sc*Sec62, *Tl*Sec62 is better resolved such that we could register amino acids to its TM1.

Sec62 forms a V-shaped structure

Sec62 consists of a cytosolic, globular N-terminal domain (NTD), two TMs (TM1 and TM2) connected by a short ER lumenal loop (L1/2), and a cytosolic C-terminal segment (Fig. 1d). Functionally essential regions have previously been mapped to the two TMs and a segment of ~30 amino acids immediately following TM2 (ref. {Wittke, 2000 #28}). The TMs of Sec62 are arranged as a V shape in front of the lateral gate with L1/2 directed to the lateral gate opening (Fig. 1a–d). The contact with the channel is mainly formed by an interaction of Sec62-TM1 with TM3 and the N-terminal segment of Sec61α.

Following TM2, Sec62 contains an oval-shaped structure lying flat on the membrane interface (Fig. 1a–d, and Extended Data Fig 3a–b). This amphipathic structure, which we termed the anchor domain, is most likely formed by an ~20-residue-long conserved segment within the abovementioned 30 amino acids, and is rich in hydrophobic amino acids (Supplementary Fig. 1). While single-point mutations of these hydrophobic residues caused no growth defect, alanine substitutions of three consecutive residues in positions 215–220 were lethal (Extended Data Fig. 3d), suggesting that decreased hydrophobicity interrupts its functionally essential interaction with the membrane. The structure of a *Tl*Sec mutant (Δanchor *Tl*Sec) with the anchor domain replaced with a glycine/serine linker showed virtually no visible Sec62 features (Extended Data Fig. 3e,f), suggesting that Sec62 becomes too mobile without the domain. Taken together, these observations suggest that the function of the anchor domain is to properly position the V-shaped TMs of Sec62 at the lateral gate.

The revealed position and topology of Sec62 raise an important question about how the channel would engage with substrate polypeptides. During the initial stage of post-translational translocation, a substrate

polypeptide is expected to insert into the channel as a loop with both its N- and C- termini exposed to the cytosol{Shaw, 1988 #82} (Extended Data Fig. 4a). While the N-terminal signal sequence may sit initially at the lateral gate as seen in structures of mammalian co-translational and bacterial post-translational complexes{Li, 2016 #40;Voorhees, 2016 #41;Ma, 2019 #70}, later it must engage with the signal peptidase for cleavage{Paetzel, 2002 #83}. Although the exact timing of the signal sequence cleavage remains unknown, the presence of Sec62 might pose a problem in this step because it may block the release of the signal sequence from the lateral gate or prevents the signal peptidase from accessing the cleavage site. The answer may be provided by a conformational transition from C1 to C2 as visualized in the *Sc*Sec structure (Fig. 1e). While in both structures the seam between the Sec62-TM1 and Sec61α-TM3 is tight, a sufficient gap is formed on the other side of the lateral gate between the Sec62-TM2 and Sec61α-TM7 in the *Sc*Sec[C2] structure. A similar gap also exists in the *Tl*Sec structures (Extended Data Fig. 4b). Thus, the signal sequence of the substrate may exit through the gap transiently formed between Sec62-TM2 and Sec61α-TM7 during translocation.

Sec62 regulates the gates of Sec61

Three distinct classes of *Sc*Sec (i.e., C1, C2, and Sec62−) showed notable conformational differences in the lateral gate (Fig. 2a, Supplementary Movie 1). Although open in all three structures, the extent of the lateral gate opening varies on the ER lumenal side, with C1 most open and Sec62− least open. The C2 structure, in which Sec62-TM2 is disengaged, is open to an intermediate degree. The movement is mainly mediated by a rigid-body rotation of the TM7, TM8, and the intervening loop (L7/8) of Sec61α (Fig. 2a), which seems to be induced by the interaction between L1/2 of Sec62 and the lateral gate (Fig. 1a–d). Thus, this movement is distinct from the hinge-like motion between the two halves (TM1–5 and TM6–10) of Sec61α which mediates opening of the channel from the fully closed state{Van den Berg, 2004 #1;Egea, 2010 #45;Park, 2014 #72;Pfeffer, 2015 #63}.

Importantly, the motion of TM7–8 of Sec61α appears to control the position of the plug (Fig. 2 b–e). In *Sc*Sec[Sec62−], the plug is clearly visible immediately below the pore constriction ('plug-closed' conformation; Fig. 2 b,d, Extended Data Fig. 5). By contrast, in *Sc*Sec[C1], the plug is displaced to a position near the C-terminus of Sec61γ ('plug-open' conformation; Fig. 2 c,e), thus opening the pore. The position of the plug in this conformation is consistent with the previous observations that the plug can interact with TM of the SecE (a prokaryotic equivalent of Sec61γ) subunit{Flower, 1995 #107;Harris, 1999 #108}. In *Sc*Sec[C2], the plug seems disordered, probably because it takes intermediate positions between the two conformations. Similar observations were also made with the *Tl*Sec structures: compared with the Sec62− and ΔSec62 structures, the Sec62+ structure shows a shifted position of Sec61α TM7–8 as in *Sc*Sec[C2] (Extended Data Fig. 6) and concomitant plug mobilization, where 53% and 42% particles classified into the plug- closed and open conformations, respectively (Extended Data Figs. 2 and 6b,c). The plug displacement is likely caused by the Sec62-induced movement of Sec61α TM7 since the plug interacts with TM7 and L7/8 in the plug-closed conformation{Egea, 2010 #45;Hizlan, 2012 #109} (Extended Data Fig. 6e).

Partially open Sec61 is inactive

Despite the observed channel gating by Sec62, physiological importance of this role remained unclear. Without Sec62, the lateral gate can still be opened by Sec63. Even though the pore is blocked by the plug, it has been proposed that insertion of a substrate polypeptide would push the plug away{Wu, 2019 #71}. To investigate importance of the Sec62-dependent gating, we sought for mutations affecting Sec61 gating as ΔSec62 does, but independently of Sec62. If the gating function of Sec62 is essential, such mutations would be expected to compromise cell viability.

We first chose to mutate the fibronectin III (FN3) domain of Sec63, which interacts with the cytosolic loop 6/7 (L6/7) of Sec61α (Fig. 3a). L6/7 also provides a major interaction site for the ribosome in cotranslational translocation and the SecA ATPase in bacterial post-translational translocation and thus has been universally implicated in priming or activating the channel{Cheng, 2005 #66;Becker, 2009 #65;Voorhees, 2014 #23;Zimmer, 2008 #22;Tsukazaki, 2008 #21}. We found that none of the FN3 mutants had a growth defect at 30°C (Fig. 3b, left). Only a mild defect was seen at 37°C even with the most severe mutant (FN3mut) (Extended Data Fig. 7b). To understand this unexpectedly weak phenotype, we determined the structure of FN3mut *Sc*Sec (Fig. 3d,e, Table 2, and Extended Data Fig. 7c,d). The structure showed that the FN3 domain was indeed disengaged from L6/7 by the mutation, causing ~10° rotation of Sec61 along the membrane normal (Extended Data Fig. 7e,f). Nonetheless, the lateral gate was still open (Fig. 3d). Importantly, the FN3mut complex still exhibited Sec62-induced TM7 movement and plug mobilization (Fig. 3 d,e), which may explain the near-WT growth phenotype of the mutant.

Next, we mutated the pore of Sec61α. In closed SecY structures{Van den Berg, 2004 #1;Tsukazaki, 2008 #21;Voorhees, 2014 #23;Tanaka, 2015 #73}, the aliphatic amino acids lining the pore constriction (called the pore ring residues) make a hydrophobic interaction with the plug. Compared to other species, the pore ring of *Sc*Sec61α appears significantly less hydrophobic{Itskanov, 2019 #69}. Thus, we reasoned that a mutant with a more hydrophobic pore ring (M90L/T185I/M294I/M450L; collectively denoted PM) might bias the plug towards the closed conformation. In growth complementation assays, PM itself did not affect cell growth. However, strong synthetic growth impairment was observed when combined with FN3mut (Fig. 3b, right). Importantly, a plug deletion{Junne, 2006 #75} (ΔPlug) could rescue growth of the FN3mut/PM, suggesting that the growth inhibition originates from a gating defect (Fig. 3c). Consistent with this idea, the structures of the combined mutant (FN3mut/PM) showed a strong density of the plug in the closed position and no Sec62-dependent movement of lateral gate helices (Fig. 3f,g, and Extended Data Fig. 7g). This conformation thereby closely resembles the gating state of *Sc*Sec[Sec62−] despite the presence of Sec62 in front of the lateral gate. On the other hand, the structure of PM alone still showed Sec62-mediated movements in the lateral gate and plug, similar to WT (Extended Data Fig. 7h,i). Taken together, these results show that the channel conformation seen in the absence of Sec62 is inactive for post-translational translocation.

Sec62 prevents invasion of lipids into the channel

In addition to the role in channel gating, the ΔSec62 *Tl*Sec structure suggests another function of Sec62—preventing lipids from moving into the channel. In ΔSec62 *Tl*Sec, strong, well-ordered densities of lipid or detergent tails are visible at the lateral gate (Fig. 4a). The densities are vertically aligned along the hydrophobic groove of the open lateral gate (Fig. 4a and Extended Data Fig. 8a). By contrast, in the Sec62+ structures, only weak fragmented densities were observed (Fig. 4b). In the cytosolic leaflet, a lipid/detergent molecule seems to be accommodated with an outward rotation of the TM2–3 of Sec61α (Extended Data Fig. 8b). Sec62 may inhibit lipids from entering the lateral gate by restricting this movement. In the ER lumenal leaflet, the L1/2 of Sec62 seems to sterically block lipids from entering (Fig. 4b). We did not observe a strong lipid/detergent density in the lateral gate of *Sc*Sec[Sec62−], perhaps because of a lower affinity to lipid/detergent. However, one of the previous *Sc*Sec structures{Wu, 2019 #71}, the conformation of which resembles the ΔSec62 *Tl*Sec structure, has shown a lipid-like density at the lateral gate and the movement of Sec61α TM2–3 similarly to ΔSec62 *Tl*Sec (Extended Data Fig. 8c,d). Collectively, these observations suggest that in the absence of Sec62, lipid molecules may penetrate the lateral gate that is opened by Sec63.

To further investigate a role of Sec62 in blocking lipid penetration, we performed 200-ns all-atom MD simulations (Fig. 4 c–h and Extended Data Fig. 9). In simulations of the Sec62-containing structures (i.e.,

WT *Tl*Sec[Sec62+/plug-open] and WT *Sc*Sec[C1] and [C2]), the translocation pore largely remained unobstructed and devoid of lipids (Fig. 4c,f, Extended Data Fig. 9 a–d, and Supplementary Movies 2–4). Only one phospholipid molecule partially penetrated the lateral gate in the cytosolic leaflet of the membrane, although its aliphatic tails remained outside; further incursion is unlikely as the interior of the cytosolic half of the channel is highly polar. Notably, no lipids penetrated the channel in the lumenal leaflet during the entire duration of the simulations, despite a larger opening (~20 Å in *Tl*Sec and ~30 Å in *Sc*Sec) between TM3 and TM7 of Sec61α (Fig. 4f, and Extended Data Fig. 9b,d). Because the plug is displaced in these structures, the lumenal funnel of Sec61α remained completely unoccupied. By contrast, simulations of the Sec62-lacking structures (ΔSec62 *Tl*Sec and *Sc*Sec[Sec62−]) showed substantially deeper penetration of lipid molecules into the lateral gate (Fig. 4 d,g, Extended Data Fig. 9e,f, and Supplementary Movies 5 and 6). In both the cytosolic and lumenal leaflets of the membrane, the lateral gate became occupied with lipids within ~80 ns. These results are consistent with the lipid/detergent densities seen in the cryo-EM structure of ΔSec62 *Tl*Sec.

Our cryo-EM structures and MD simulations suggested that the V-shaped transmembrane domain of Sec62 effectively blocks lipids from entering the open lateral gate, particularly on the ER lumenal leaflet. We thus hypothesized that without Sec62, the pore may be invaded by lipids if both lateral gate and plug remain open. We tested this idea by running another set of MD simulations on *Tl*Sec[Sec62+] and *Sc*Sec[C1] but excluding the Sec62 subunit (Fig. 4e,h, Extended Data Fig. 9c,f, Supplementary Movies 7 and 8). The results indeed show that in both *Tl*Sec and *Sc*Sec, lipids invaded into the pore, substantially obstructing the translocation pathway. It is likely that lipid molecules occupying the pore would inhibit insertion of substrate polypeptides. Thus, Sec62 seems to play an important role in maintaining the functionality of Sec61 by keeping lipids away from the open channel.

Mechanism of Sec61 gating by Sec63

One unexpected finding was that the FN3–L6/7 interaction was dispensable for the protein translocation function of the Sec complex. This indicates that there must be another mechanism for Sec63 to open the lateral gate. Besides the FN3 domain, Sec63 forms major contacts with Sec61 through two other parts: TM3, which anchors Sec63 to the Sec61 complex, and a short ER lumenal segment (residues 210–216) preceding the TM3, which together with the N-terminal segment of Sec63, interacts with a crevice on the back of the channel (opposite from the lateral gate) (Fig. 5a). We reasoned that the latter interaction might control lateral gating through a lever-like mechanism. In the WT background, replacement of this segment with a glycine/serine linker (Δ210-216) alone did not cause growth inhibition (Fig. 5b). However, when combined with FN3mut, cells did not grow (Fig. 5b).

To understand the structural basis of this synthetic defect, we determined the structure of the FN3mut/Δ210-216 *Sc*Sec complex (Fig. 5c and Extended Data Fig. 10) The structure showed that indeed both the lateral and vertical gates of the Sec61 channel are completely closed, resembling the idle archaeal SecY channel structure{Van den Berg, 2004 #1} (Fig. 5c and Extended Data Fig. 10). This demonstrates that Sec63 uses both its cytosolic and lumenal domains to open the lateral gate in a two-pronged mechanism. The C-terminal cytosolic domain of Sec63 (following TM3) and Sec71–Sec72 are still attached to Sec61 through TM3. However, most of the parts preceding TM3 were invisible due to increased flexibility. Importantly, Sec62 was no longer visible either despite copurification with the complex (Fig. 5c, and Extended Data Fig. 10a). Sec62 is likely associated with Sec63 through an electrostatic interaction with the C-terminal tail of Sec63 (ref.{Wittke, 2000 #28;Willer, 2003 #29}) (Fig. 1d), but it seems to no longer bind to the lateral gate due to structural incompatibility with the closed gate. Therefore, the lateral gate must be first opened by Sec63 before Sec62 can activate the channel for protein translocation.

Discussion

In summary, our study defines the functions of Sec62 and reveals the mechanism by which Sec63 and Sec62 regulate the gates of the Sec61 channel. The function of Sec62 had been elusive for three decades since its discovery as an essential component in eukaryotic post-translational translocation{Deshaies, 1989 #62;Rothblatt, 1989 #9;Deshaies, 1991 #8}. Our study shows that once the lateral gate of the Sec61 channel is opened by Sec63, Sec62 fully activates the channel by further mobilizing the plug domain (Fig. 6). At the same time, Sec62 seems to prevent lipids from penetrating the channel interior through the open lateral gate by forming a barrier in front of the lateral gate. Such lipid penetration into the lateral gate and translocation pore would likely impair the protein translocation activity by competitively inhibiting insertion of polypeptide substrates into the channel. The lipids may also affect movements of polypeptides in later stages of protein translocation. The V-shaped structure formed by the transmembrane domain of Sec62 is rather dynamic with respect to the rest of the complex and loosely associated with the lateral gate, as suggested by its relatively low-resolution densities in our cryo-EM maps. This flexibility may be important for insertion of signal sequences into and its egress from the lateral gate. It is also possible that the movement of Sec62 is modulated by binding of signal sequences and other protein translocation factors (e.g., BiP) to the Sec61 channel.

The fully open conformation of the WT Sec complexes observed in our cryo-EM structures likely represents a resting state prior to substrate engagement. Although the channel's conformation and their dynamics in the native membrane environment remains to be determined, we speculate that this open state is likely a predominant form in the native ER membrane at least in fungal species, based on the stable association between Sec61, Sec62, and Sec63. A pre-opened Sec61 channel in the post-translational complex contrasts with a relatively closed Sec61 channel seen with resting co-translational complexes, where the lateral gate is only marginally open, and the plug domain remains in the closed position {Voorhees, 2014 #23}. It has been generally thought that during initial substrate engagement, the Sec61 channel would be opened by a hydrophobic interaction between the signal sequence (or TM helix) and the lateral gate{Gogala, 2014 #87;Voorhees, 2014 #23;Voorhees, 2016 #3;Voorhees, 2016 #41;Kater, 2019 #88}. Our mutagenesis analysis however indicates that such a partially open state, like the one induced by Sec63 alone, is insufficient for post-translational protein translocation. This is probably because the plug domain in the closed position would impose a too high energy barrier for post-translational polypeptide substrates to insert into the pore.

Many post-translational substrates are known to contain a signal sequence with relatively lower hydrophobicity{Ng, 1996 #5}. Eukaryotic post-translational substrates are also expected to interact more transiently with Sec61 during initial insertion because they are not tethered to the ribosome as in the co-translational mode or the SecA ATPase as in the bacterial post-translational mode. These features of substrates for the Sec complex may require both lateral and vertical gates of the channel to be pre-opened for efficient insertion. A reduced energy barrier for substrate insertion by pre-opening the gates would allow polypeptides to promptly engage with the Sec61 complex, without which polypeptides may lose translocation competency because of premature folding or aggregation. Maintaining a stably open conformation by Sec63 and Sec62 may also be important for subsequent translocation steps as it may reduce friction in polypeptide movements. Our structural analysis shows that Sec63 and Sec62 open the gates of the Sec61 channel in a stepwise fashion to activate the channel, explaining their essentiality in cell viability. Given the high degree of sequence conservation of these components, the gating mechanism we discovered here is likely conserved across all eukaryotic species.

Acknowledgments

We thank D. Toso and J. Remis for support for electron microscope operation, and J. Hurley and E. Nogales for critical reading of manuscript. This work was supported by the Vallee Scholars Program (E.P.) and the National Institutes of Health (J.C.G.; R01-GM123169). Computational resources were provided through the Extreme Science and Engineering Discovery Environment (XSEDE; TG-MCB130173), which is supported by a National Science Foundation Grant (ACI-1548562). Additional resources were provided by the Partnership for an Advanced Computing Environment (PACE) at the Georgia Institute of Technology.

Author contributions

S.I. prepared samples and performed functional analysis. S.I. and E.P. collected and analyzed cryo-EM data, built atomic models, interpreted results. K.M.K and J.C.G performed MD simulations and interpret results, and E.P. supervised the project and wrote the manuscript with input from all authors.

Competing interests

The authors declare no competing interests.

Data and materials availability:

The atomic coordinates and cryo-EM density maps of the Sec complexes were deposited to the Protein Data Bank (PDB) and Electron Microscopy Data Bank (EMDB), respectively. Their PDB and EMDB accession codes are as follows: EMD-22785 for *Sc*Sec[consensus]; 7KAH and EMD-22770 for *Sc*Sec[Sec62−]; 7KAI and EMD-22771 for *Sc*Sec[C1]; 7KAJ and EMD22772 for *Sc*Sec[C2]; 7KAO and EMD-22778 for PM *Sc*Sec[Sec62−]; 7KAP and EMD-22779 for PM *Sc*Sec[C1]; 7KAQ and EMD-22780 for PM *Sc*Sec[C2]; 7KAR and EMD-22781 for FN3mut *Sc*Sec[Sec62−]; 7KAS and EMD-22782 for FN3mut *Sc*Sec[Sec62+]; 7KAT and EMD-22783 for PM/FN3mut *Sc*Sec[Sec62−]; 7KAU and EMD-22784 for PM/FN3mut *Sc*Sec[Sec62+]; 7KB5 and EMD-22787 for FN3mut/Δ210-216 *Sc*Sec; EMD-22786 for WT *Tl*Sec[Sec62+]; 7KAK and EMD-22773 for *Tl*Sec[Sec62−]; 7KAL and EMD-22774 for *Tl*Sec[Sec62+/plug-open]; 7KAM and EMD-22775 for *Tl*Sec[Sec62+/plug-closed]; 7KAN and EMD-22776 for ΔSec62 *Tl*Sec; EMD-22777 for Δanchor *Tl*Sec. Yeast strains and plasmids that were generated in this study are available upon request.

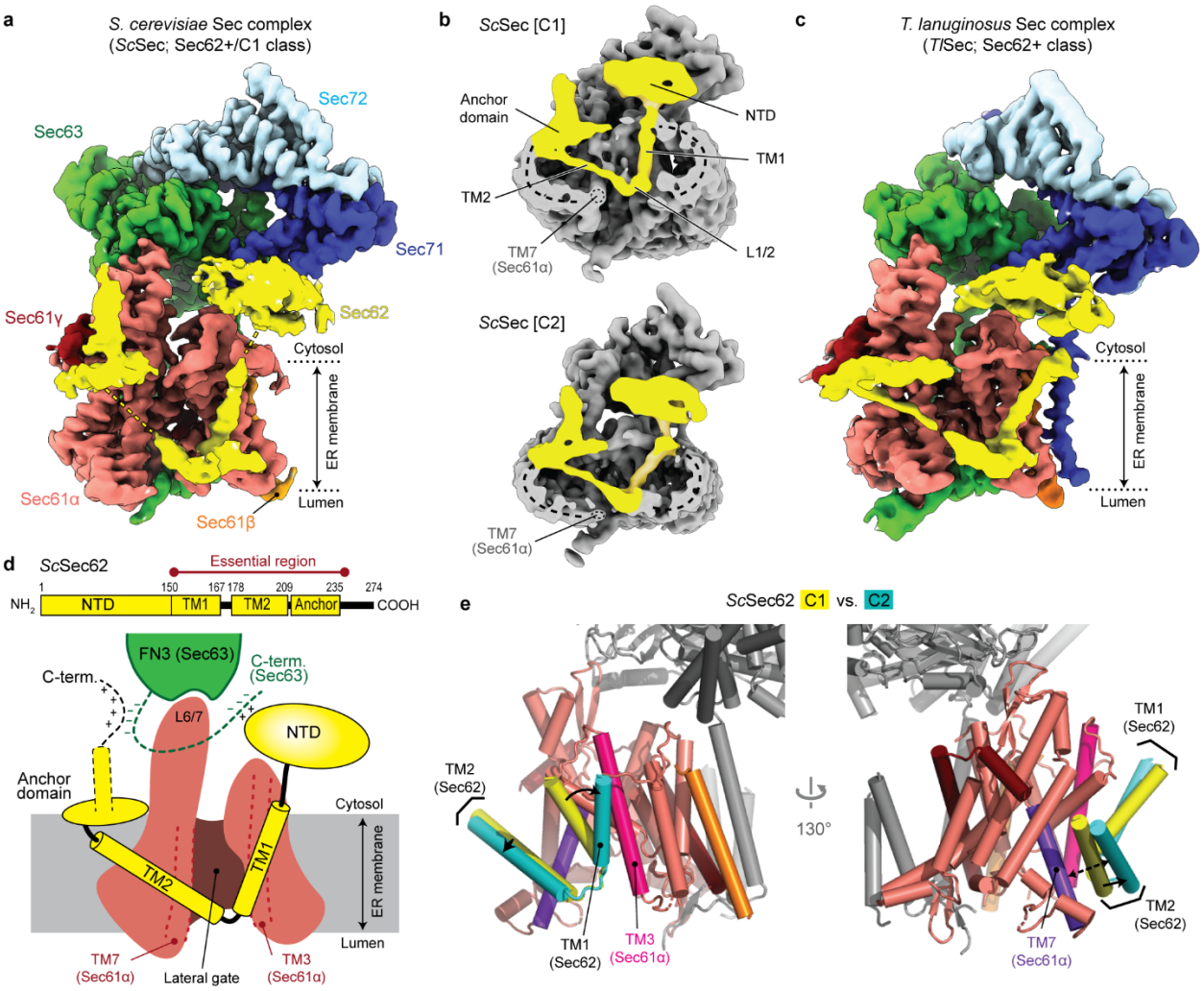

Figure 1. Cryo-EM analysis of fungal Sec complexes and the structure of Sec62. **a**, The 3.1-Å-resolution cryo-EM reconstruction of the yeast Sec complex (C1 class, front view into the lateral gate). Yellow dash lines indicate the connections that are visible at a lower contour level (see panel b). In yeast nomenclature, the α, β, and γ subunits of the Sec61 complex are called Sec61p, Sbh1p, and Sss1p, respectively. **b**, Cutaway views showing Sec62 (yellow). Shown are 6-Å-lowpass-filtered C1 (upper panel; a tilted view from the ER lumen) and C2 (lower panel; front view) maps. Dashed line, detergent micelle. **c**, The 3.8-Å-resolution reconstruction of the *T. lanuginosus* Sec complex (the consensus Sec62+ map). **d**, Domain organization of Sec62. Previous studies suggest an interaction between the NTD of Sec62 and the C-terminal tail of Sec63 (ref. {Wittke, 2000 #28;Willer, 2003 #29}). In addition, based on the proximity, the C-terminal tails of Sec62 and Sec63 may also interact with each other through an electrostatic interaction. **e**, Interactions between the Sec62 TMs and lateral gate. Dashed arrow, a gap between Sec61α TM7 and Sec62 TM2 in the C2 conformation. Sec61α is in salmon with its TM3 and TM7 in magenta and violet, respectively. Sec61β and Sec61γ are in orange and dark red, respectively. Sec62 is in yellow (C1) or cyan (C2). Sec63, Sec71, and Sec72 are in grey.

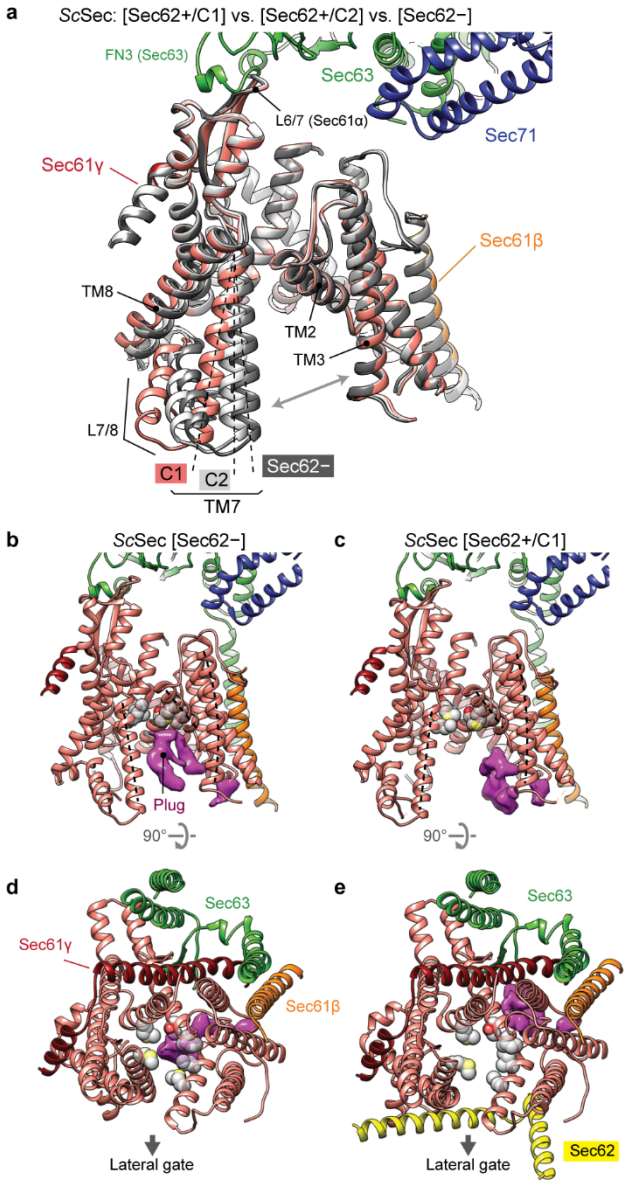

Figure 2. Regulation of the lateral and vertical gates by Sec62. **a**, A comparison of the Sec61 channel conformation between the three *Sc*Sec classes, C1 (in color), C2 (light grey) and Sec62− (dark grey). Dashed lines, TM7 of Sec61α. Grey arrows, the lateral gate. Sec62 is not shown. **b**–**e**, A comparison of the plug domain (purple density) between Sec62-lacking and -containing *Sc*Sec classes. Grey spheres, pore ring residues. Dashed lines, lateral gate helices (left to right: TM7, TM2, and TM3 of Sec61α). Shown are front views (b and c) and cytosolic views (d and e).

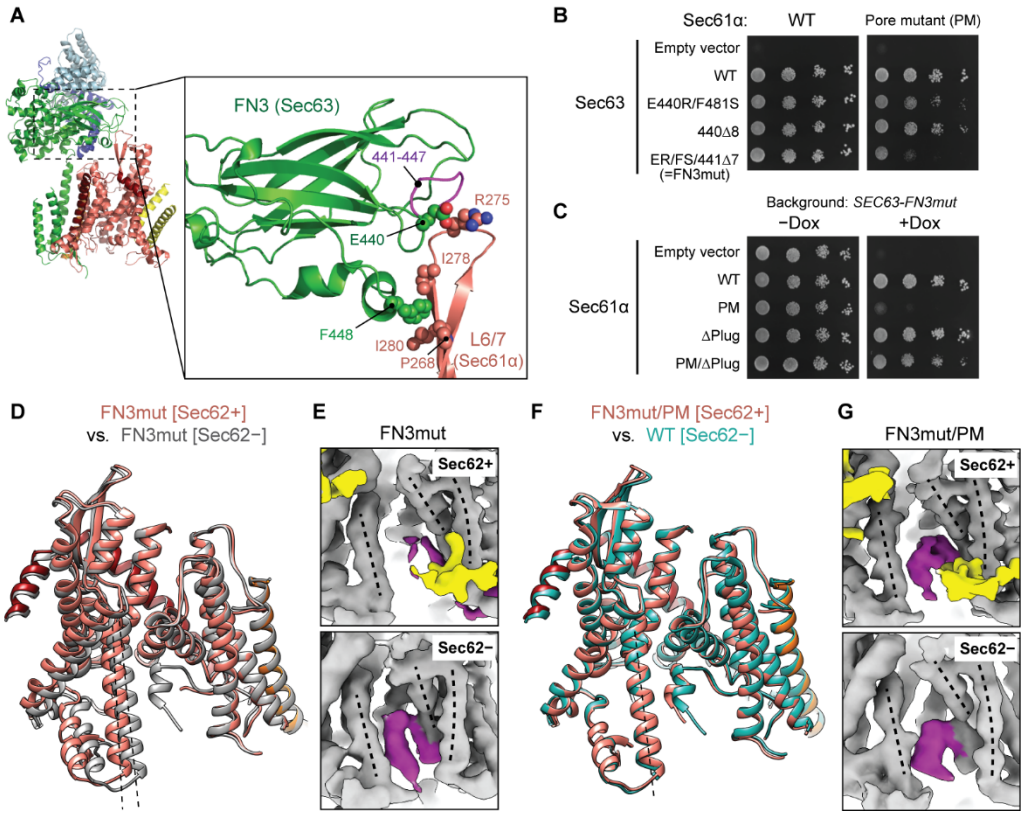

Figure 3. Structural and functional analysis of a gating-defective mutant complex. a, The interaction between the FN3 domain of Sec63 and the L6/7 loop of Sec61α (shown is WT *Sc*Sec[C1]). Amino acids involved in the interactions are indicated. **b**, Yeast growth complementation experiments (at 30°C) testing functionality of indicated FN3 mutants of Sec63 in the background of WT (left) or pore-mutant (PM) Sec61α (right). FN3mut refers to a combination of E440R (ER) and F481S (FS) mutations and a deletion of seven amino acids 441–447 (441Δ7). To repress chromosomal WT Sec63 expression (under a tetracycline promoter), doxycycline was added. Also see Extended Data Fig. 7a. **c**, As in b, but testing for indicated Sec61α mutants in the background of Sec63-FN3mut as a sole Sec63 copy. The addition of doxycycline (Dox) represses chromosomal WT Sec61α expression. **d**, As in Fig. 2a, but with the FN3mut *Sc*Sec structures with and without Sec62. **e**, A comparison of the plug domain (purple density) between the FN3mut *Sc*Sec structures with and without Sec62 (yellow). Dashed lines, lateral gate helices (left to right: TM7, TM2, and TM3 of Sec61α). **f**, As in d, but comparing the Sec62-containing FN3mut/PM structure and the Sec62− class of WT *Sc*Sec. **g**, As in e, but with the FN3mut/PM *Sc*Sec structures.

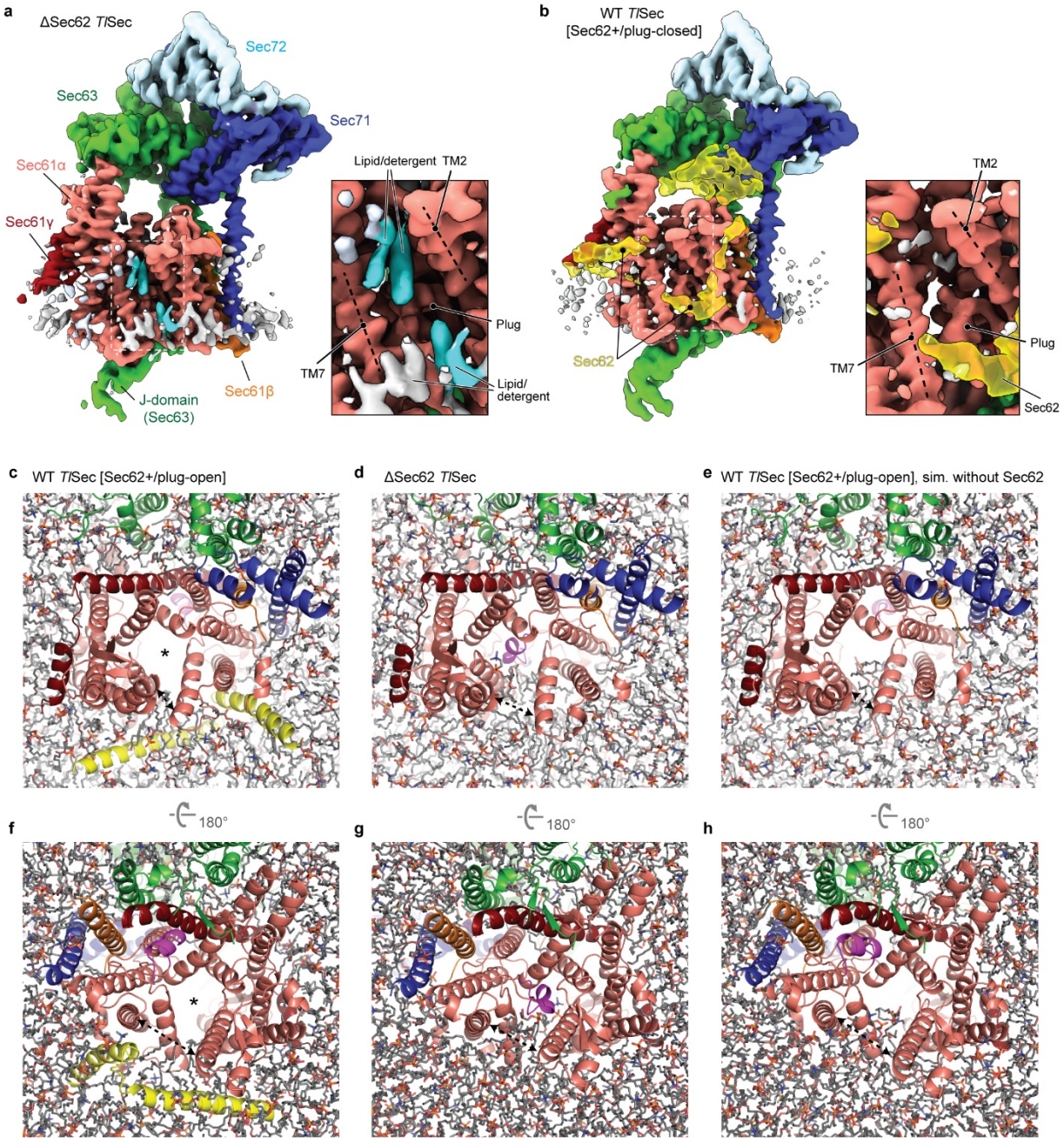

Figure 4. Sec62 prevents lipids from invading into the Sec61 channel. **a**. Lipid/detergent molecules at the lateral gate in the *Tl*Sec structure lacking Sec62 (ΔSec62). The left panel is a front view. Non-protein densities are in grey. Densities in cyan are lipid/detergent molecules intercalated at the lateral gate. The right panel is a zoomed-in view of the lateral gate (area indicated by the white dashed box in the left panel). **b**, As in a, but with the Sec62+/plug-closed class of WT *Tl*Sec. We note that similarly, the Sec62+/plug-open class does not show lipid/detergent densities at the lateral gate. **c**–**h**. All-atom MD simulations with indicated *Tl*Sec structures in a model membrane. The Sec complex is shown in a ribbon representation in the same colors as in a and b. Lipids are shown in a stick representation. Panels c–e are views from the cytosol, and f–h are views from the ER lumen. In c and f, the translocation pore is marked by an asterisk. The lateral gate openings are indicated by a dashed arrow. The frames are from 200 ns after the initiation of simulations.

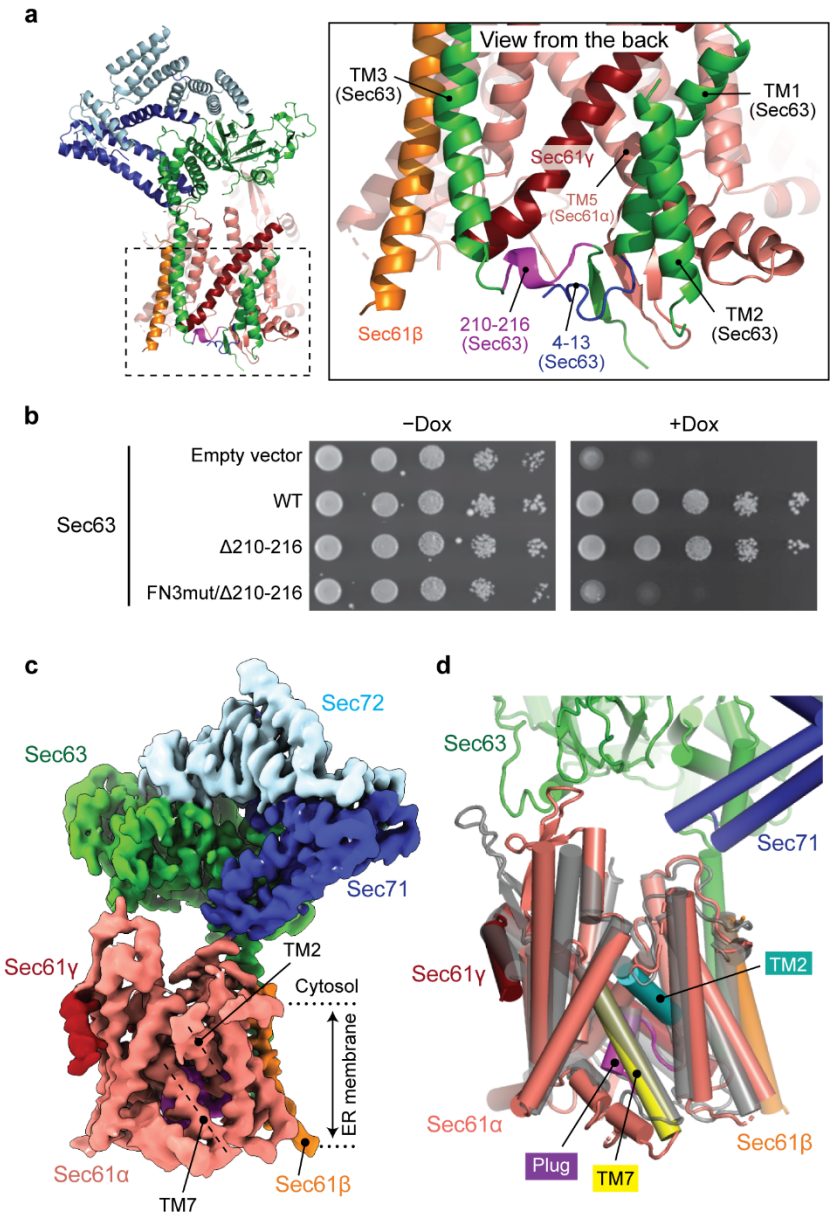

Figure 5. The structure of a fully closed Sec complex. **a**, The interaction between Sec61 and Sec63 in the ER lumen (view from the back). The N-terminal segment (positions 4–13) and the segment preceding TM3 (positions 210–216) of Sec63 are in blue and purple, respectively. Shown is the *Sc*Sec[C1] structure. **b**, Yeast growth complementation (at 30°C) testing functionality of the indicated Sec63 mutants. The addition of doxycycline (Dox) represses chromosomal WT Sec63 expression. **c**, The 3.8-Å-resolution cryo-EM structure of the *Sc*Sec complex containing FN3mut/Δ210-216 double-mutant Sec63. The lateral gate helices TM2 and TM7 are indicated. **d**, As in c, but showing the atomic model of the Sec61 complex. For comparison, the closed *M. jannaschii* SecY structure (PDB 1RH5; semitransparent grey) is superimposed.

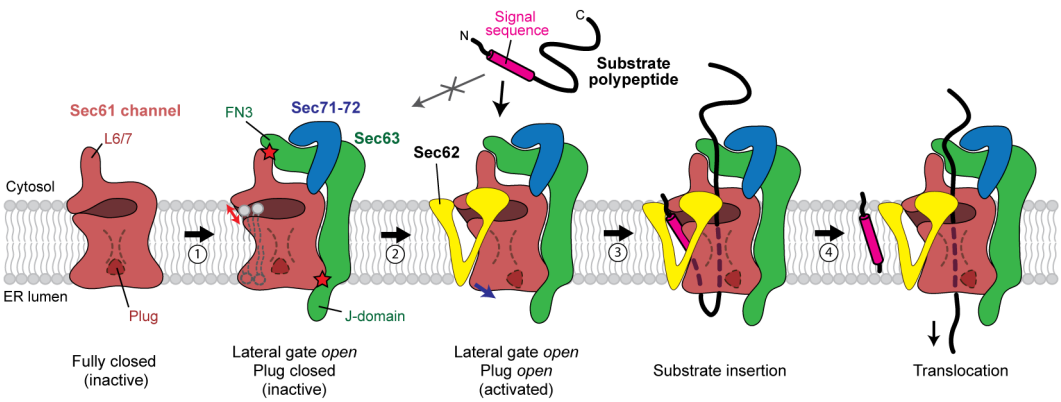

Figure 6. A model for activation of the Sec61 channel by Sec62 and Sec63. The Sec61 channel alone assumes a fully closed conformation (the leftmost cartoon). Step 1, association of Sec63 opens the lateral gate (indicated by a red arrow) through interactions with Sec61 in both the cytosol and ER lumen (indicated by red stars). However, the channel in this conformation is inactive due to the plug in a closed state. In addition, without Sec62, lipids may enter the open lateral gate. Step 2, Sec62 interacts with the lateral gate of Sec61 and further opens the lateral gate (blue arrow), which results in opening of the plug. The V-shaped transmembrane domain of Sec62 excludes lipids from the channel. Step 3, a substrate polypeptide inserts into the open pore of the channel as a loop with the signal sequence sitting at the lateral gate. Step 4, The signal sequence is cleaved by the signal peptidase (not shown), and the polypeptide is translocated into the ER lumen. For simplicity, the BiP ATPase, which drives translocation by interactions with the polypeptide and J-domain, is not shown.

Table 1. Cryo-EM data collection, refinement and validation statistics of wildtype *Sc*Sec and wildtype and mutant *Tl*Sec complexes

	Wildtype *Sc*Sec			Wildtype *Tl*Sec			ΔSec62 *Tl*Sec	Δanchor *Tl*Sec
	Sec62−	Sec62+/C1	Sec62+/C2	Sec62−	Plug-open	Plug-closed		
EM Databank accession code	22770	22771	22772	22773	22774	22775	22776	22777
PDB accession code	7KAH	7KAI	7KAJ	7KAK	7KAL	7KAM	7KAN	N/A
Data collection								
Magnification	42,017x			43,860x			43,860x	42,017x
Voltage (kV)	300			200			200	300
Electron exposure (e^-/Å^2)	49.1			50.0			50.0	49.1
Defocus range (μm)	-0.8 to -2.5			-0.6 to -2.4			-0.9 to -2.2	-0.7 to -2.9
Pixel size (Å)	1.19			1.14			1.14	1.19
Processing								
Symmetry imposed	C1	C1	C1	C1	C1	C1	C1	C1
Initial particle images (no.)	2,686,839			1,632,659			546,712	229,825
Final particle images (no.)	391,885	193,263	193,661	155,601	114,704	143,227	222,047	76,726
Map resolution (Å)	3.1	3.2	3.1	3.9	4.0	3.8	3.7	4.4
FSC threshold	0.143	0.143	0.143	0.143	0.143	0.143	0.143	0.143
Map resolution range (Å)	2.6 – 11	2.8 – 12	2.7 – 12	3.4 – 13	3.3 – 13	3.3 – 12	3.3 – 12	3.7 – 14
Refinement								
Initial model used (PDB code)	6N3Q	WT *Sc*Sec [Sec62-]	WT *Sc*Sec [Sec62-]	ΔSec62 *Tl*Sec	ΔSec62 *Tl*Sec	ΔSec62 *Tl*Sec	6N3Q	-
Model resolution (Å)	3.2	3.3	3.3	4.1	4.2	4.0	4.0	-
FSC threshold	0.5	0.5	0.5	0.5	0.5	0.5	0.5	-
Map sharpening *B* factor (Å^2)	86.6	80.8	75.9	110.3	90.7	105.2	127.8	-
Model composition								
Nonhydrogen atoms	10,495	10,718	10,712	10,438	10,794	10,921	10,661	-
Protein residues	1,349	1,399	1,399	1,371	1,429	1,445	1,371	-
Ligands	-	-	-	-	-	-	2 (PC2)	
B factors, average (Å^2)	73	61	58	117	126	74	30	-
R.m.s. deviations								
Bond lengths (Å)	0.003	0.003	0.003	0.002	0.002	0.003	0.003	-
Bond angles (°)	0.522	0.508	0.513	0.524	0.489	0.521	0.623	-
Validation								
MolProbity score	1.43	1.42	1.33	1.51	1.42	1.48	1.55	-
Clashscore	4.61	4.14	3.87	6.33	5.62	5.60	6.18	-
Poor rotamers (%)	0	0	0	0	0	0	0	-
Ramachandran plot								
Favored (%)	96.83	96.58	97.01	97.09	97.42	96.96	96.72	-
Allowed (%)	3.17	3.42	2.99	2.91	2.58	3.04	3.28	-
Disallowed (%)	0	0	0	0	0	0	0	-